The skeleton of tropical intraseasonal oscillations

Andrew J. Majda[a,1] and Samuel N. Stechmann[b]

[a]Department of Mathematics and Center for Atmosphere Ocean Science, Courant Institute of Mathematical Sciences, New York University, New York, NY 10012; and [b]Department of Mathematics and Department of Atmospheric and Oceanic Sciences, University of California, Los Angeles, CA 90095

Contributed by Andrew J. Majda, March 26, 2009 (sent for review February 27, 2009)

The Madden–Julian oscillation (MJO) is the dominant mode of variability in the tropical atmosphere on intraseasonal timescales and planetary spatial scales. Despite the primary importance of the MJO and the decades of research progress since its original discovery, a generally accepted theory for its essential mechanisms has remained elusive. Here, we present a minimal dynamical model for the MJO that recovers robustly its fundamental features (i.e., its "skeleton") on intraseasonal/planetary scales: (*i*) the peculiar dispersion relation of $d\omega/dk \approx 0$, (*ii*) the slow phase speed of ≈5 m/s, and (*iii*) the horizontal quadrupole vortex structure. This is accomplished here in a model that is neutrally stable on planetary scales; i.e., it is tacitly assumed that the primary instabilities occur on synoptic scales. The key premise of the model is that modulations of synoptic scale wave activity are induced by low-level moisture preconditioning on planetary scales, and they drive the "skeleton" of the MJO through modulated heating. The "muscle" of the MJO—including tilts, vertical structure, etc.—is contributed by other potential upscale transport effects from the synoptic scales.

Madden–Julian oscillation | convectively coupled equatorial waves | atmospheric convection

The dominant component of intraseasonal variability in the tropics is the 40- to 50-day tropical intraseasonal oscillation, often called the Madden–Julian oscillation (MJO) after its discoverers (1, 2). In the troposphere, the MJO is an equatorial planetary-scale wave envelope of complex multi-scale convective processes. It begins as a standing wave in the Indian Ocean and propagates eastward across the western Pacific Ocean at a speed of ≈5 m/s (3). The planetary-scale circulation anomalies associated with the MJO significantly affect monsoon development, intraseasonal predictability in midlatitudes, and the development of the El Niño southern oscillation (ENSO) in the Pacific Ocean, which is one of the most important components of seasonal prediction (3, 4).

Despite the widespread importance of the MJO, present-day computer general circulation models (GCMs) typically have poor representations of it (5). A growing body of evidence suggests that this poor performance of GCMs is due to the inadequate treatment of interactions of organized tropical convection on multiple spatiotemporal scales (5, 6). Such hierarchical organized structures that generate the MJO as their envelope are the focus of current observational initiatives and modeling studies (6), and there is a general lack of theoretical understanding of these processes and the MJO itself.

A large number of theories have attempted to explain the MJO through mechanisms such as evaporation–wind feedback (7, 8), boundary layer frictional convective instability (9), stochastic linearized convection (10), radiation instability (11), and the planetary-scale linear response to moving heat sources (12). While they all provide some insight into the mechanisms of the MJO, these theories are all at odds with the observational record in various crucial ways (3, 4), and it is therefore likely that none of them captures the fundamental physical mechanisms of the MJO. Nevertheless, they are all interesting theories that contribute to our understanding of certain aspects of the MJO. Other insight has been gained through the study of MJO-like waves in multicloud model simulations (13, 14) and in superparameterization computer simulations (15–18), which appear to capture many of the observed features of the MJO by accounting for smaller-scale convective structures within the MJO envelope. The role of convective momentum transport from synoptic scale waves in producing key features of the MJO's planetary scale envelope has also been elucidated by multiscale asymptotic models (19–23). Despite all of the interesting contributions listed above, no theory for the MJO has yet been generally accepted, and the problem of explaining the MJO has recently been called the search for the Holy Grail of tropical atmospheric dynamics (11). Here, we contribute to this search.

Although theory and simulation of the MJO remain difficult challenges, they are guided by the generally accepted, fundamental features of the MJO (i.e., the MJO's "skeleton") on intraseasonal/planetary scales, which have been identified relatively clearly in observations:

I. Peculiar dispersion relation of $d\omega/dk \approx 0$ (24–26),
II. Slow phase speed of roughly 5 m/s (27–29), and
III. Horizontal quadrupole vortex structure (27–29).

The goal of this article is to design the simplest dynamical model that captures the intraseasonal/planetary scale features I–III of the MJO's "skeleton", and to recover these features robustly throughout the parameter space of the model.

Physical Mechanisms and Basis of the Model

Many previous attempts at a theory for the MJO emphasize different planetary scale instability mechanisms as being fundamental to its existence (7–12). Here, instead, the premise is that the intraseasonal/planetery skeleton of the MJO in I–III arises through neutrally stable interactions. The tacit assumption is that the primary instabilities and damping occur on synoptic scales (30–32), and the "muscle" of the MJO is provided by convective momentum transport from synoptic scale waves (19–23) and enhanced surface heat fluxes (33). The fundamental mechanism proposed here for the MJO skeleton involves neutrally stable interactions between (*i*) planetary scale, lower tropospheric moisture anomalies and (*ii*) synoptic scale convectively coupled wave activity, whose modulations provide the planetary scale heating anomalies that drive the planetary scale circulation.

Several studies have shown that the lower troposphere tends to moisten during the suppressed convection phase of the MJO, and lower tropospheric moisture appears roughly in quadrature with the MJO's heating anomaly (34–36). It is well-known that this low-level moisture content plays a key role in regulating mesoscale convection, and there is a growing body of evidence that shows it also plays a key role in regulating convection on the scales of synoptic scale convectively coupled waves and the MJO (13, 14, 31, 32, 34–36). A fundamental part of the model presented below is the effect of low-level moisture on the envelope of synoptic scale wave activity.

Author contributions: A.J.M. and S.N.S. designed research, performed research, and wrote the paper.

The authors declare no conflict of interest.

Freely available online through the PNAS open access option.

[1]To whom correspondence should be addressed. E-mail: jonjon@cims.nyu.edu.

The important role of synoptic scale wave activity in driving the MJO is documented in a growing body of evidence in the form of observations (28, 37, 38), simulations (13–17, 23), and theory (18–22). This synoptic scale wave activity is a complex menagerie of convectively coupled equatorial waves, such as 2-day waves, convectively coupled Kelvin waves, etc. (30–32), and it drives the MJO in 2 main ways. First, the planetary scale MJO skeleton is driven by modulated heating anomalies from the planetary scale modulations of the synoptic scale wave activity (20). Second, the "muscle" of the MJO is provided by convective momentum transport from vertically tilted synoptic scale waves, which drives the MJO's westerly wind burst (18–20, 22, 23), and by enhanced surface heat fluxes (33).

Several previous diagnostic models for the MJO have illuminated some of its basic planetary scale features. Matsuno–Gill models show a basic Kelvin–Rossby wave structure for the MJO (39, 40), although it lacks the horizontal quadrupole vortices. This model has been refined by also including 3 cloud types (instead of only one) in creating the mean planetary scale heating (20). Here, we formulate a dynamic version of a Matsuno–Gill model with the important distinction that there is no dissipation on planetary scales; i.e., convective momentum transport does not create mean damping on intraseasonal/planetary scales. This is in accordance with evidence that convective momentum transport can sometimes accelerate and sometimes decelerate the mean wind on intraseasonal/planetary scales (19, 20, 23, 41, 42). In fact, no prominent large-scale dissipative mechanisms are included in the model here except a fixed, constant radiative cooling. The tacit assumption is that the primary instabilities occur on synoptic scales (30–32). In short, the flavor of Matsuno–Gill models is retained here, except there are no dissipative mechanisms, and the dynamic heating arises from modulations of synoptic scale wave activity, which respond to anomalies of lower tropospheric moisture.

The Dynamic Model

Here, based on the mechanisms outlined in the previous section, a dynamic model is designed for the MJO skeleton on intraseasonal/planetary scales. The model is formulated in terms of anomalies from a uniform base state of radiative–convective equilibrium, $\bar{R} = \bar{H}\bar{a}$, where $\bar{R} = 1$ K/d is the fixed, constant radiative cooling rate, $\bar{H}$ is a constant heating rate prefactor, and $\bar{a}$ is a constant (nondimensional) amplitude of wave activity in the equilibrium state. The dry dynamical core of the model is the equatorial long-wave equations (19–21, 43), and 2 other dynamic variables are included to represent moist convective processes:

$$\begin{aligned} q &: \text{lower tropospheric moisture} \\ a &: \text{amplitude of wave activity envelope} \end{aligned} \qquad [1]$$

The nondimensional dynamical variable a parameterizes the amplitude of the planetary scale envelope of synoptic scale wave activity. It is noteworthy that, for the MJO skeleton model designed here, it is only the amplitude of the wave activity envelope that is needed, not any of the details of the particular synoptic scale waves (30–32) that make up the envelope. A key aspect of the model here is the interaction between a and q: as motivated by the discussion in the previous section, positive (negative) low-level moisture anomalies create a tendency to enhance (decrease) the envelope of equatorial synoptic scale wave activity. The simplest equation for the wave activity with these features is $a_t = \Gamma q(\bar{a} + a)$. The wave activity envelope then feeds back on the other variables through a heat source $\bar{H}a$ and—in accordance with conservation of moist static energy—a moisture sink $-\bar{H}a$. Thus the model equations for the anomalies from radiative–convective equilibrium take the form

$$\begin{aligned} u_t - yv &= -p_x \\ yu &= -p_y \\ 0 &= -p_z + \theta \\ u_x + v_y + w_z &= 0 \\ \theta_t + w &= \bar{H}a \\ q_t - \tilde{Q}w &= -\bar{H}a \\ a_t &= \Gamma q(\bar{a} + a). \end{aligned} \qquad [2]$$

Here, u, v, and w are the zonal, meridional, and vertical velocities, respectively; and p and θ are the pressure and potential temperature, respectively. Notice that this model contains a minimal number of parameters: $\tilde{Q} = 0.9$, the (nondimensional) mean background vertical moisture gradient; and $\Gamma = 1$, where Γq acts as a dynamic growth/decay rate of the wave activity envelope in response to moisture anomalies. In dimensional units, $\Gamma \approx 0.2\ \mathrm{K}^{-1}\ \mathrm{d}^{-1}$. These will be the standard parameter values used here unless otherwise noted. Also notice that the parameter $\bar{H}$ is actually irrelevant to the dynamics (as can be seen by rescaling Eq. **2** and recalling the equilibrium condition $\bar{R} = \bar{H}\bar{a}$), but it is written here for clarity of presentation.

Vertical and Meridional Truncation. Now, we introduce the simplest dynamical model that looks like the Matsuno–Gill model plus low-level moisture advection and wave activity. To obtain this model from Eq. **2**, first linearize the a equation and truncate the vertical structures at the first baroclinic mode:

$$\begin{aligned} u_t - yv - \theta_x &= 0 \\ yu - \theta_y &= 0 \\ \theta_t - u_x - v_y &= \bar{H}a \\ q_t + \tilde{Q}(u_x + v_y) &= -\bar{H}a \\ a_t &= \Gamma\bar{a}q. \end{aligned} \qquad [3]$$

Note that the variables in Eq. **3** have first baroclinic mode vertical structures [either $\cos(z)$ or $\sin(z)$] associated with them (21, 43), and a slight abuse of notation has been made in keeping the same variable labels in Eq. **3** as in Eq. **2**.

The next step in obtaining the simplest dynamical model for the MJO skeleton is to assume that the modulated heating due to synoptic scale wave activity has the simple equatorial meridional structure proportional to $\exp(-y^2/2)$. Such a meridional heating structure is known to excite only Kelvin waves and the first symmetric equatorial Rossby waves (21, 43), and one can write the resulting meridionally truncated equations as

$$\begin{aligned} K_t + K_x &= -\frac{1}{\sqrt{2}}\bar{H}A \\ R_t - \frac{1}{3}R_x &= -\frac{2\sqrt{2}}{3}\bar{H}A \\ Q_t + \frac{1}{\sqrt{2}}\tilde{Q}K_x - \frac{1}{6\sqrt{2}}\tilde{Q}R_x &= \left(-1 + \frac{1}{6}\tilde{Q}\right)\bar{H}A \\ A_t &= \Gamma\bar{a}Q \end{aligned} \qquad [4]$$

where K and R are the amplitudes of the Kelvin and equatorial Rossby waves, respectively, and they have the associated meridional structures as shown in Fig. 1. In the absence of forcing, the "dry" long-wave Kelvin and equatorial Rossby wave solutions of Eq. **4** are dispersionless waves that propagate at 50 and 17 m/s, respectively (21, 43). In the presence of the dynamical forcing A in Eq. **4**, the Kelvin and equatorial Rossby waves can be coupled to each other and to Q and A, and these coupled modes can

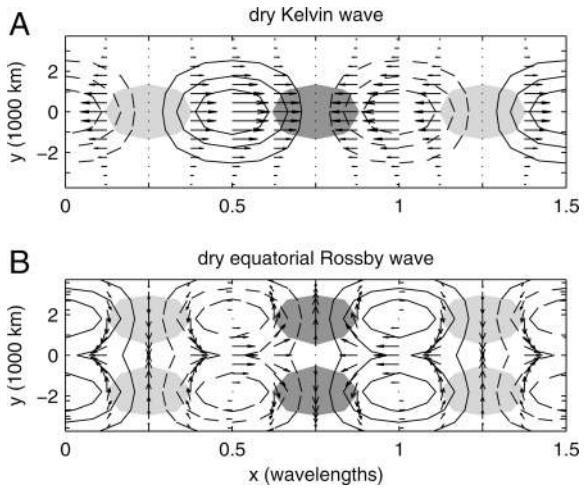

Fig. 1. Physical structures of the unforced "dry" Kelvin wave (*A*) and equatorial Rossby wave (*B*) obtained from Eq. **6**. Contours show lower tropospheric pressure with positive (negative) anomalies denoted by solid (dashed) lines. The contour interval is one-fourth the maximum amplitude of the anomaly, and the zero contour is not shown. Anomalies of convergence (divergence) that are greater than two-thirds the maximum amplitude are shaded dark (light) gray.

be dispersive. Both Q and A have associated meridional structures proportional to $\exp(-y^2/2)$. A higher meridional mode of moisture is also excited by this simple equatorial heating, and it evolves as

$$\partial_t q_2 + \tilde{Q}\left(-\frac{1}{12}R_x + \frac{1}{3\sqrt{2}}\bar{H}A\right) = 0, \qquad [5]$$

where q_2 has an associated meridional structure proportional to $(2y^2-1)\exp(-y^2/2)$, and it does not feed back onto the variables K, R, Q, A (i.e., it is slaved to them) because of the assumed meridional truncation of a. The variables u, v, θ are then recovered by using the formulas (21, 43)

$$\begin{aligned} u &= \frac{1}{\sqrt{2}}\left(K - \frac{1}{2}R\right)\phi_0 + \frac{1}{4}R\phi_2 \\ \theta &= -\frac{1}{\sqrt{2}}\left(K + \frac{1}{2}R\right)\phi_0 - \frac{1}{4}R\phi_2 \\ v &= \left(\frac{1}{3}R_x - \frac{1}{3\sqrt{2}}\bar{H}A\right)\phi_1, \end{aligned} \qquad [6]$$

where $\phi_0 \propto \exp(-y^2/2)$, $\phi_1 \propto y\exp(-y^2/2)$, and $\phi_2 \propto (2y^2-1)\exp(-y^2/2)$ are the parabolic cylinder functions that yield the meridional structures of the variables (21, 43). Thus, the linear equations in Eq. **4** provide the simplest dynamical model for the MJO skeleton by implementing a Matsuno–Gill model plus low-level moisture advection and equatorial wave activity.

Formula for Intraseasonal Oscillation Frequency. A formula for the intraseasonal oscillation frequency ω of the MJO skeleton can be obtained by considering the even simpler case of flow above the equator. In this case, Eq. **3** is used, v and y are set to zero, and meridional derivatives are ignored. The result is a linear system of four equations for u, θ, q, a, and the system can be solved exactly due to the perfect east–west symmetry:

$$2\omega^2 = \Gamma\bar{R} + k^2 \pm \sqrt{(\Gamma\bar{R}+k^2)^2 - 4\Gamma\bar{R}k^2(1-\tilde{Q})} \qquad [7]$$

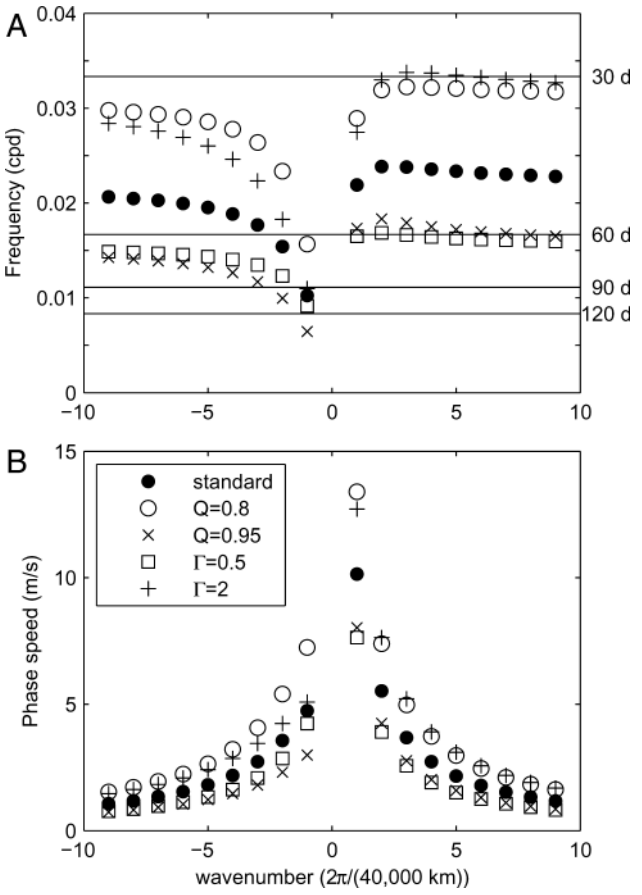

Fig. 2. Linear wave oscillation frequency $\omega(k)$ (*A*) and phase speed ω/k (*B*) as functions of wavenumber k for the low-frequency modes of Eq. **4**. Filled circles denote results with the standard parameter values. Other markers denote results with one change made to the standard parameter values: $\tilde{Q} = 0.8$ (open circles), $\tilde{Q} = 0.95$ (crosses), $\Gamma = 0.5$ (squares), and $\Gamma = 2$ (pluses). Horizontal lines in *A* denote oscillation periods of 30, 60, 90, and 120 days.

where k is the zonal wavenumber. A simple formula for the oscillation frequency of the low-frequency waves,

$$\omega \approx \sqrt{\Gamma\bar{R}(1-\tilde{Q})}, \qquad [8]$$

can be obtained from Eq. **7** approximately. For the standard parameter values used here, the oscillation period corresponding to Eq. **8** is 45 days, in agreement with observations of the MJO (24–26). Notice that this formula is independent of the wavenumber k; i.e., this model recovers the peculiar dispersion relation $d\omega/dk \approx 0$ from the observational record (24–26).

The approximate formula in Eq. **8** is valid provided that $\epsilon_1 = 4\Gamma\bar{R}k^2(1-\tilde{Q})(\Gamma\bar{R}+k^2)^{-2} \ll 1$ and $\epsilon_2 = \Gamma\bar{R}k^{-2} \ll 1$. For the standard parameter values used here, the nondimensional numbers ϵ_1 and ϵ_2 are, in fact, significantly less than 1. The value of ϵ_1 is roughly 4×10^{-4} for wavenumber 1; and the value of ϵ_2 is 0.4 for wavenumber 1, 0.1 for wavenumber 2, and even smaller for higher wavenumbers. Thus, the approximations $\epsilon_1 \ll 1$ and $\epsilon_2 \ll 1$ are valid, and it will be shown below that Eq. **8** holds for the eastward-propagating branch of the beta-plane model Eq. **4** as well.

The Skeleton of the MJO

In this section, the linear waves of the simplest model in Eqs. **4**–**6** are presented. Because Eq. **4** involves 4 dynamically coupled

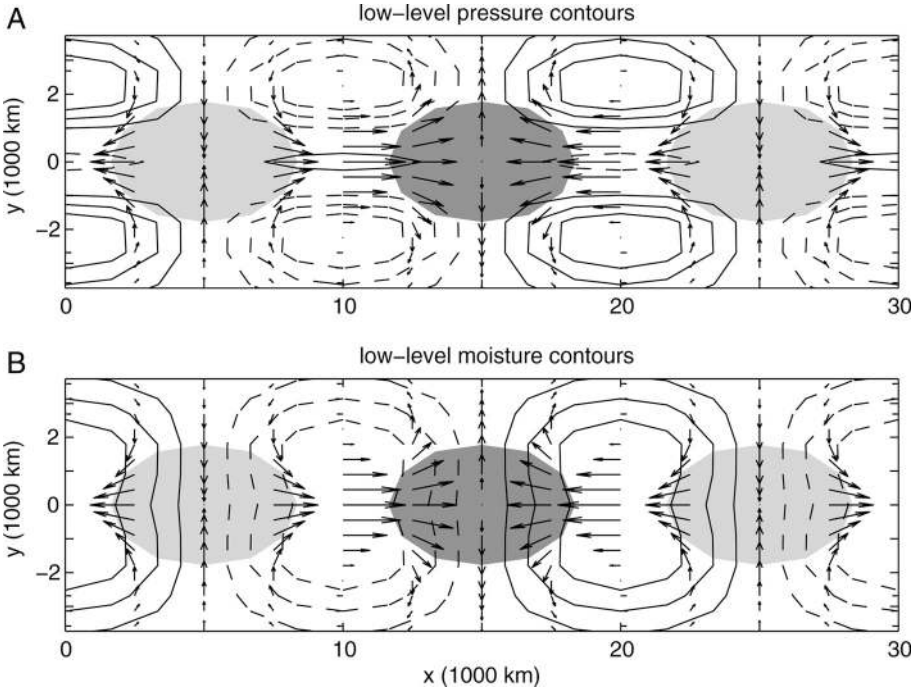

Fig. 3. Physical structure of the wavenumber-2 MJO mode of Eqs. **4**–**6** for the standard parameter values. Lower tropospheric velocity vectors are shown with contours of lower tropospheric pressure anomalies (*A*) and lower tropospheric moisture anomalies (*B*) with positive (negative) anomalies denoted by solid (dashed) lines. The contour interval is one-fourth the maximum amplitude of the anomaly, and the zero contour is not shown. Positive (negative) anomalies of wave activity *A* that are greater than one-half the maximum amplitude are shaded dark (light) gray.

variables, there are 4 linear modes. The dispersion relation for the linear modes is shown in Fig. 2. (Only the 2 low-frequency, intraseasonal modes are shown. The other 2 modes are high-frequency modes and are only weakly coupled to the wave activity; they will be discussed only briefly below.) Fig. 2 shows that eastward-propagating waves, like the MJO (24–26), have the peculiar dispersion relation $d\omega/dk \approx 0$. Moreover, this dispersion relation is robust over a wide range of parameter values, and the oscillation periods spanned by these reasonable parameter values are in the range of 30–60 days, which is the observed range of the MJO's oscillation period (24–26). The westward-propagating waves, however, which are plotted with positive ω and negative k, have variable ω, and their oscillation periods are seasonal, not intraseasonal, for $k = 1$ and 2. This suggests the first piece of our explanation for the observed dominance of eastward-propagating intraseasonal variability: the westward-propagating modes have seasonal oscillation periods, on which timescales other phenomena are expected to dominate over modulations of synoptic scale wave activity.

The physical structure of the wavenumber-2 MJO mode is shown in Fig. 3 for the standard parameter values. Horizontal quadrupole vortices are prominent, as in observations (27–29), and the maximum wave activity is colocated with the maximum in equatorial convergence. The lower tropospheric moisture leads and is in quadrature with the wave activity, which is also roughly the relationship seen in observations (34–36). The pressure contours clearly display the mixed Kelvin/Rossby wave structure of the wave. Equatorial high-pressure anomalies are colocated with the westerly wind burst as in Kelvin waves; and they are flanked by off-equatorial low-pressure anomalies and cyclonic Rossby gyres, in broad agreement with the observational record (27–29). Rectification of the vertical structure and some of the phase relationships is likely due to effects of higher vertical modes (13, 14, 19, 20).

The relative contributions of K, R, Q, and A to these linear waves are shown in Fig. 4 for wavenumbers 1, 2, and 3. The MJO has significant contributions from both the Kelvin and Rossby components, whereas the westward modes are dominated by the Rossby component. In addition, the larger Q and A amplitudes suggest further explanation for eastward-propagating rather than westward-propagating intraseasonal oscillations: the eastward-propagating modes are more strongly coupled to equatorial moist convective processes.

The sensitivity of the wave structure to parameter changes is shown in Table 1. The wave structures are robust over a wide range of parameter values. Changes are generally less than 10% for K, R, and A, whereas Q shows changes of as much as 30% from its standard value.

The physical structure of the wavenumber-2 low-frequency westward-propagating mode is shown in Fig. 5. Its circulation is almost purely Rossby wave-like with little character of a Kelvin wave, and the positive anomaly of low-level moisture preconditioning is confined closely to the vicinity of the equator. This wave differs from observed convectively coupled equatorial Rossby waves in several respects, such as its equatorial (as opposed to off-equatorial) heating anomaly, low frequency, and slow propagation speed (30, 44–46). However, the spectral filters used for the wave structures in these observational studies tend to emphasize relatively high spatiotemporal frequencies, whereas the spectral peaks tend to occur on wavenumbers 3–5 with oscillation periods of 20–60 days (25, 26, 30, 46). The present models do capture features of the observed westward spectral peak for these wavenumbers.

In addition to the low-frequency modes presented above, the simplest linear model in Eq. **4** also has 2 high-frequency modes (not shown). The eastward- and westward-propagating high-frequency modes propagate at 50–60 m/s and 17–30 m/s, respectively, and, relative to the low-frequency modes, they are only weakly coupled to the wave activity A. For these and other reasons, the high-frequency modes do not appear to be related to observed convectively coupled equatorial waves (30, 32). They have phase

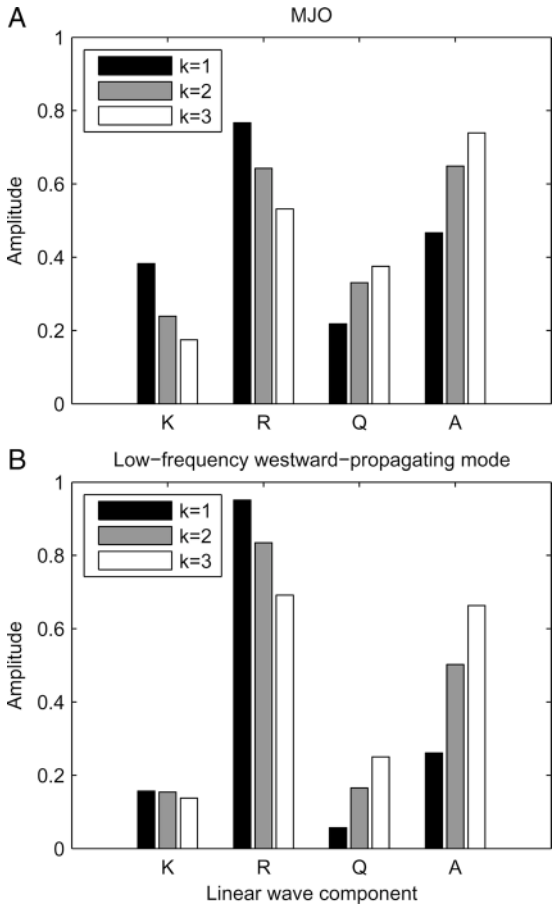

Fig. 4. Contributions of each component K, R, Q, and A to the linear wave eigenvectors of the MJO (A) and the low-frequency westward-propagating mode (B) for the standard parameter values. Results for wavenumbers $k = 1, 2$, and 3 are shown in black, gray, and white, respectively.

speeds comparable to the dry Kelvin and equatorial Rossby waves, and they passively carry a small moisture trace.

Concluding Discussion

A new minimal dynamical model for the MJO was presented that recovers robustly its fundamental features (i.e., its "skeleton") on intraseasonal/planetary scales:

I. Peculiar dispersion relation of $d\omega/dk \approx 0$,
II. Slow phase speed of roughly 5 m/s, and
III. Horizontal quadrupole vortex structure.

Table 1. Sensitivity of low-frequency wave structure to changes in model parameters

k	$\tilde{Q}$	Γ	K	R	Q	A
+2	0.90	1.0	0.24	0.64	0.33	0.65
+2	0.80	1.0	0.25	0.58	0.44	0.64
+2	0.95	1.0	0.23	0.68	0.25	0.65
+2	0.90	0.5	0.21	0.64	0.43	0.60
+2	0.90	2.0	0.27	0.63	0.24	0.69
−2	0.90	1.0	0.15	0.83	0.17	0.50
−2	0.80	1.0	0.13	0.86	0.22	0.45
−2	0.95	1.0	0.17	0.82	0.11	0.54
−2	0.90	0.5	0.16	0.80	0.27	0.51
−2	0.90	2.0	0.15	0.85	0.10	0.49

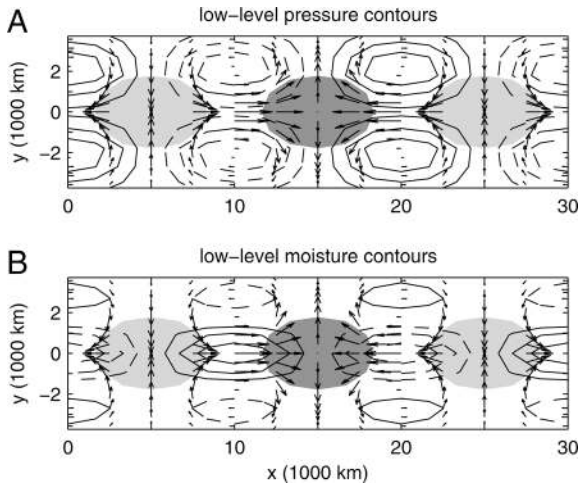

Fig. 5. Physical structure of the wavenumber-2 low-frequency westward mode of Eqs. **4**–**6**. Plots are drawn as in Fig. 3.

In addition, the simple formula

$$\omega \approx \sqrt{\Gamma \bar{R}(1-\tilde{Q})} \qquad [9]$$

for the roughly constant oscillation frequency of the MJO was derived, and the model displays east/west asymmetry on intraseasonal/planetary scales that is consistent with the observational record. The key premise of the model is that modulations of synoptic scale wave activity are induced by low-level moisture preconditioning, and they drive the "skeleton" of the MJO through modulated heating. The "muscle" of the MJO—including tilts, vertical structure, etc.—is contributed by other upscale transports from the synoptic scales. The model was designed with neutrally stable interactions on intraseasonal/planetary scales, with the tacit assumption that the primary instabilities in the tropical atmosphere occur on synoptic scales.

The model was designed to capture the fundamental features of the MJO on intraseasonal/planetary scales in the simplest setting. Additional aspects of the vertical and meridional structure of the MJO could be obtained by including additional vertical and meridional modes, and the "muscle" of the MJO could be included through active convective momentum transports and enhanced surface heat fluxes. Nonlinear simulations of the model would also reveal additional physical effects beyond the basic linear theory shown here.

The simplest model shown here suggests an explanation for the observed dominance of eastward-propagating intraseasonal variabilility: the eastward-propagating modes are more strongly coupled with the equatorial moist convective processes, and the westward modes occur on seasonal time scales for wavenumbers 1 and 2. The westward-propagating modes are dominated by the Rossby wave contribution over the Kelvin wave contribution, and they share some features with observed convectively coupled equatorial Rossby waves, but the simplest model considered here did not include all of the physical processes that appear to be necessary from observations. For instance, off-equatorial convection and the barotropic mode appear to play an important role in convectively coupled equatorial Rossby waves, and these processes could be included in the future.

ACKNOWLEDGMENTS. This work was supported in part by National Science Foundation Grants DMS–0456713 and ONR N0014–08–0284 (to A.J.M.) and by a National Oceanic and Atmospheric Administration Climate and Global Change Postdoctoral Fellowship (to S.N.S.).

1. Madden R, Julian P (1971) Detection of a 40-50 day oscillation in the zonal wind in the tropical Pacific. *J Atmos Sci* 28:702–708.
2. Madden RA, Julian PR (1994) Observations of the 40-50-day tropical oscillation—A review. *Mon Weather Rev* 122:814–837.
3. Zhang C (2005) Madden–Julian Oscillation. *Rev Geophys* 43:G2003.
4. Lau WKM, Waliser DE, eds. (2005) *Intraseasonal Variability in the Atmosphere—Ocean Climate System* (Springer, Berlin).
5. Lin JL, et al. (2006) Tropical intraseasonal variability in 14 IPCC AR4 climate models. Part I. Convective signals. *J Climate* 19:2665–2690.
6. Moncrieff MW, Shapiro M, Slingo J, Molteni F (2007) Collaborative research at the intersection of weather and climate. *WMO Bull* 56:204–211.
7. Emanuel KA (1987) An air-sea interaction model of intraseasonal oscillations in the Tropics. *J Atmos Sci* 44:2324–2340.
8. Neelin JD, Held IM, Cook KH (1987) Evaporation-wind feedback and low-frequency variability in the tropical atmosphere. *J Atmos Sci* 44:2341–2348.
9. Wang B, Rui H (1990) Dynamics of the coupled moist Kelvin-Rossby wave on an equatorial beta-plane. *J Atmos Sci* 47:397–413.
10. Salby ML, Garcia RR, Hendon HH (1994) Planetary-scale circulations in the presence of climatological and wave-induced heating. *J Atmos Sci* 51:2344–2367.
11. Raymond DJ (2001) A new model of the Madden–Julian oscillation. *J Atmos Sci* 58:2807–2819.
12. Chao WC (1987) On the origin of the tropical intraseasonal oscillation. *J Atmos Sci* 44:1940–1949.
13. Majda AJ, Stechmann SN, Khouider B (2007) Madden–Julian oscillation analog and intraseasonal variability in a multicloud model above the equator. *Proc Natl Acad Sci USA* 104:9919–9924.
14. Khouider B, Majda AJ (2007) A simple multicloud parameterization for convectively coupled tropical waves. Part II. Nonlinear simulations. *J Atmos Sci* 64:381–400.
15. Grabowski WW (2001) Coupling cloud processes with the large-scale dynamics using the cloud-resolving convection parameterization (CRCP). *J Atmos Sci* 58:978–997.
16. Grabowski WW (2003) MJO-like coherent structures: sensitivity simulations using the cloud-resolving convection parameterization (CRCP). *J Atmos Sci* 60:847–864.
17. Grabowski WW, Moncrieff MW (2004) Moisture-convection feedback in the Tropics. *Q J R Meteorol Soc* 130:3081–3104.
18. Moncrieff MW (2004) Analytic representation of the large-scale organization of tropical convection. *J Atmos Sci* 61:1521–1538.
19. Majda AJ, Biello JA (2004) A multiscale model for the intraseasonal oscillation. *Proc Natl Acad Sci USA* 101:4736–4741.
20. Biello JA, Majda AJ (2005) A new multiscale model for the Madden–Julian oscillation. *J Atmos Sci* 62:1694–1721.
21. Biello JA, Majda AJ (2006) Modulating synoptic scale convective activity and boundary layer dissipation in the IPESD models of the Madden–Julian oscillation. *Dyn Atmos Oceans* 42:152–215.
22. Biello JA, Majda AJ, Moncrieff MW (2007) Meridional momentum flux and superrotation in the multi-scale IPESD MJO model. *J Atmos Sci* 64:1636–1651.
23. Majda AJ, Stechmann SN (2009) A simple dynamical model with features of convective momentum transport. *J Atmos Sci* 66:373–392.
24. Salby M, Hendon H (1994) Intraseasonal behavior of clouds, temperature, and motion in the tropics. *J Atmos Sci* 51:2207–2224.
25. Wheeler M, Kiladis GN (1999) Convectively coupled equatorial waves: analysis of clouds and temperature in the wavenumber–frequency domain. *J Atmos Sci* 56:374–399.
26. Roundy P, Frank W (2004) A climatology of waves in the equatorial region. *J Atmos Sci* 61:2105–2132.
27. Hendon HH, Salby ML (1994) The life cycle of the Madden–Julian oscillation. *J Atmos Sci* 51:2225–2237.
28. Hendon HH, Liebmann B (1994) Organization of convection within the Madden–Julian oscillation. *J Geophys Res* 99:8073–8084.
29. Maloney ED, Hartmann DL (1998) Frictional moisture convergence in a composite life cycle of the Madden–Julian oscillation. *J Climate* 11:2387–2403.
30. Kiladis GN, Wheeler MC, Haertel PT, Straub KH, Roundy PE, Convectively coupled equatorial waves. *Rev Geophys,* 47, RG2003, DOI: 10.1029/2008RG000266.
31. Khouider B, Majda AJ (2006) A simple multicloud parameterization for convectively coupled tropical waves. Part I: Linear analysis. *J Atmos Sci* 63:1308–1323.
32. Khouider B, Majda AJ (2008) Equatorial convectively coupled waves in a simple multicloud model. *J Atmos Sci* 65:3376–3397.
33. Sobel AH, Maloney ED, Bellon G, Frierson DM, Surface fluxes and tropical intraseasonal variability: a reassessment. *J Adv Model Earth Syst*, in press.
34. Kiladis GN, Straub KH, Haertel PT (2005) Zonal and vertical structure of the Madden–Julian oscillation. *J Atmos Sci* 62:2790–2809.
35. Tian B, et al. (2006) Vertical moist thermodynamic structure and spatial–temporal evolution of the MJO in AIRS observations. *J Atmos Sci* 63:2462–2485.
36. Kikuchi K, Takayabu Y (2004) The development of organized convection associated with the MJO during TOGA COARE IOP: Trimodal characteristics. *Geophys Res Lett* 31, L10101, DOI: 10.1029/2004GL019601.
37. Houze RA Jr, Chen SS, Kingsmill DE, Serra Y, Yuter SE (2000) Convection over the Pacific warm pool in relation to the atmospheric Kelvin–Rossby wave. *J Atmos Sci* 57:3058–3089.
38. Masunaga H, L'Ecuyer T, Kummerow C (2006) The Madden–Julian oscillation recorded in early observations from the Tropical Rainfall Measuring Mission (TRMM). *J Atmos Sci* 63:2777–2794.
39. Matsuno T (1966) Quasi-geostrophic motions in the equatorial area. *J Meteorol Soc Japan* 44:25–43.
40. Gill A (1980) Some simple solutions for heat-induced tropical circulation. *Q J R Meteorol Soc* 106:447–462.
41. Tung W, Yanai M (2002) Convective momentum transport observed during the TOGA COARE IOP. Part I. General features. *J Atmos Sci* 59:1857–1871.
42. Tung W, Yanai M (2002) Convective momentum transport observed during the TOGA COARE IOP. Part II. Case studies. *J Atmos Sci* 59:2535–2549.
43. Majda AJ (2003) *Introduction to PDEs and Waves for the Atmosphere and Ocean*, Courant Lecture Notes in Mathematics (American Mathematical Society, Providence, RI) Vol 9, pp. x + 234.
44. Kiladis G, Wheeler M (1995) Horizontal and vertical structure of observed tropospheric equatorial Rossby waves. *J Geophys Res* 100:22981–22998.
45. Wheeler M, Kiladis GN, Webster PJ (2000) Large-scale dynamical fields associated with convectively coupled equatorial waves. *J Atmos Sci* 57:613–640.
46. Yang G, Hoskins B, Slingo J (2007) Convectively coupled equatorial waves. Part I. Horizontal and vertical structures. *J Atmos Sci* 64:3406–3423.